Article

Experimental Mixed-Gas Permeability, Sorption and Diffusion of CO_2-CH_4 Mixtures in 6FDA-mPDA Polyimide Membrane: Unveiling the Effect of Competitive Sorption on Permeability Selectivity

Giuseppe Genduso *[ID], **Bader S. Ghanem and Ingo Pinnau** *

Functional Polymer Membranes Group, Advanced Membranes and Porous Materials Center, Division of Physical Science and Engineering, King Abdullah University of Science and Technology, Thuwal 23955-6900, Saudi Arabia; bader.ghanem@kaust.edu.sa
* Correspondence: giuseppe.genduso@kaust.edu.sa (G.G.); ingo.pinnau@kaust.edu.sa (I.P.)

check for updates

Abstract: The nonideal behavior of polymeric membranes during separation of gas mixtures can be quantified via the solution-diffusion theory from experimental mixed-gas solubility and permeability coefficients. In this study, CO_2-CH_4 mixtures were sorbed at 35 °C in 4,4′-(hexafluoroisopropylidene)diphthalic dianhydride (6FDA)-m-phenylenediamine (mPDA)—a polyimide of remarkable performance. The existence of a linear trend for all data of mixed-gas CO_2 versus CH_4 solubility coefficients—regardless of mixture concentration—was observed for 6FDA-mPDA and other polymeric films; the slope of this trend was identified as the ratio of gas solubilities at infinite dilution. The CO_2/CH_4 mixed-gas solubility selectivity of 6FDA-mPDA and previously reported polymers was higher than the equimolar pure-gas value and increased with pressure from the infinite dilution value. The analysis of CO_2-CH_4 mixed-gas concentration-averaged effective diffusion coefficients of equimolar feeds showed that CO_2 diffusivity was not affected by CH_4. Our data indicate that the decrease of CO_2/CH_4 mixed-gas diffusion, and permeability selectivity from the pure-gas values, resulted from an increase in the methane diffusion coefficient in mixtures. This effect was the result of an alteration of the size sieving properties of 6FDA-mPDA as a consequence of CO_2 presence in the 6FDA-mPDA film matrix.

Keywords: mixed-gas sorption; mixed-gas diffusion; mixed-gas permeation; competitive sorption; gas separation membranes; 6FDA-mPDA polyimide

1. Introduction

Conventional distillation or absorption and adsorption systems are reliable and, for existing plants, economically feasible technologies. However, membrane units could potentially replace these traditional unit operations, ensuring better economics and lower environmental impact [1]. To fully exploit the potential of membrane-based gas-separations, polymeric materials of high permeability and permeability selectivity are required. Moreover, these materials must be mechanically strong for formation of integral asymmetric and thin-film composite membranes and should also ensure stable separation performances over time. Currently, most experimental studies reported in the literature are based on pure-gas permeation properties of membrane materials (e.g., cellulose acetate, polysulfone, polyphenylene oxide, polyimides, polymers of intrinsic microporosity (PIM), and others) [2–6]. However, when gas permeation is performed under mixed-gas conditions, permeability and permeability selectivity can deviate significantly from the pure-gas values. For example, the pure-gas CO_2/CH_4 permeability selectivity of PIM-1 is ~15 (in the range of 0–10 atm

CO_2 pressure), but drops to ~8 in a CO_2/CH_4 mixture at 10 atm partial CO_2 pressure [4], that is, only ~50% of the ideal value. Because the overall intention of CO_2-CH_4 separation studies is to design membrane materials for industrial applications, correct identification of the reasons for the deviation from ideality of permeability selectivity is crucial. Therefore, one should describe gas transport at both thermodynamic (sorption) and kinetic (diffusion) levels. The solution-diffusion theory that is commonly applied to describe the transport of fluids through dense polymer membranes affirms that permeability (P_i) can be directly determined as the combination of solubility (S_i) and diffusion (D_i) coefficients of a specific gas in a membrane [7]. Hence, to accurately describe the transport of gases through membranes, one should preferably couple mixed-gas permeation data, measured by a well-established experimental technique [8], with mixed-gas sorption or diffusion data. Fraga et al. [9], for example, designed and implemented a new time lag apparatus for the direct measurement of mixed-gas permeability and diffusion coefficients in Pebax 2533, HyflonAD60X, and PIM-EA-TB—the same instrument was used by Monteleone et al. [10] to test mixed-gas diffusion coefficients of a spirobifluorene-based polymer of intrinsic microporosity (PIM-SBF-1). On the basis of our experimental capabilities, we estimated mixed-gas diffusion coefficient values by applying the solution-diffusion theory and combining experimental mixed-gas permeability and mixed-gas sorption values. Particularly, a newly developed sorption system was used for the mixed-gas sorption studies reported here [11]. To the best of our knowledge, so far, four types of mixed-gas sorption units have been described in the literature [11–15] and utilized to test a total of only 11 polymers [11–23]. Furthermore, the number of studies covering the diffusion of gas mixtures in polymers—retrieved from experiments of mixed-gas sorption and permeation—is even smaller. Some previous studies include the following: CO_2-C_2H_6 in XLPEO [24], n-C_4H_{10}-CH_4 in poly [1-trimethylsilyl-1-propyne] (PTMSP) [25], CO_2-CH_4 in 6FDA-TADPO [22], CO_2-CH_4 in PEO-based multi-block copolymer [26], n-C_4H_{10}-CH_4 in polydimethylsiloxane (PDMS) [27], and CO_2-CH_4 in PDMS [11]. In our previous work [11], we showed that co-permeation of CO_2 in mixtures with CH_4 in rubbery polydimethylsiloxane (PDMS) increased mixed-gas diffusion of CH_4.

Similar to other commercial glassy polymers (e.g., polysulfones, cellulose acetates), polyimides have attracted the attention of the academic and industrial community for the following reasons: (i) strong thermal and mechanical properties (high glass transition and thermal decomposition temperatures, high ultimate tensile strength/elongation at break, and Young's modulus) and (ii) excellent combination of pure-gas permeability and permeability selectivity [5]. In particular, polyimides based on the commercially available monomer 4,4′-(hexafluoroisopropylidene)diphthalic dianhydride (6FDA) are typically solution processable and, therefore, suitable for hollow fibers spinning [5,28]. The polycondensation reaction of 6FDA with m-phenylenediamine (mPDA)—a commercially available monomer—yields the high-performance 6FDA-mPDA polyimide [29,30], shown in Figure 1. 6FDA-mPDA displays an interesting combination of pure-gas CO_2 permeability of ~14 Barrer and CO_2/CH_4 permeability selectivity of ~70 measured at 2 atm and 35 °C [27]. Therefore, this membrane material is a particularly attractive polymer to perform a case study of mixed-gas sorption and diffusion of CO_2-CH_4 mixtures in polyimides. Such a study may also clarify whether the deviation of the CO_2 mixed-gas permeability from the pure-gas values can be ascribed to *competitive sorption* phenomena—as commonly assumed in the literature [31–33]—or to phenomena related to CO_2-induced dilation [34].
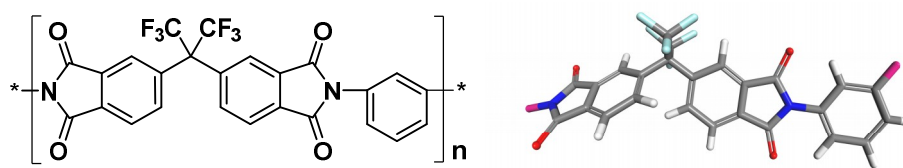
Figure 1. Chemical structure and 3D representation of the repeat unit of 4,4′-(hexafluoroisopropylidene)diphthalic dianhydride (6FDA)-m-phenylenediamine (mPDA) polyimide.

In this work, we aimed to provide a full experimental description of sorption and diffusion of CO_2-CH_4 mixtures in isotropic 6FDA-mPDA films at 35 °C. First, we show the results of CO_2-CH_4 mixed-gas sorption experiments, and then perform an analysis of mixture effects on the solubility coefficients and solubility selectivity at various equilibrium pressures. To analyze mixed-gas solubility data, isothermal surfaces of gas uptake were estimated via the following: (i) linear interpolation and (ii) the extension of the dual-mode sorption model [35] to mixtures supported by an empirical expression for better data fitting. In the second part of this work, experimental mixed-gas permeability values of 6FDA-mPDA obtained with equimolar CO_2-CH_4 mixtures previously reported by our group [29] were divided by experimental mixed-gas solubilities to estimate CO_2-CH_4 mixed-gas concentration-averaged effective diffusion coefficient data. These data show the interaction between CO_2 and the polymeric matrix of 6FDA-mPDA and the effect of CO_2 diffusion on CH_4 diffusion. Moreover, using our experimental data, we were able to clarify the impact of competitive sorption and CO_2-sorption related phenomena on transport and separation of CO_2-CH_4 mixtures in 6FDA-mPDA.

2. Materials and Methods

2.1. Materials

6FDA-mPDA was synthesized according to the procedure reported elsewhere [29]. The polymer had a weight-averaged molecular weight (Mw) of 141,000 g/mol and a polydispersity index (Mw/Mn) of 1.2. Isotropic polyimide films made by solution casting from chloroform were air-dried, soaked in methanol for 12 h, and then dried at 120 °C under vacuum for 24 h. Complete solvent removal was confirmed by thermal gravimetric analysis (TGA). The geometric density of 6FDA-mPDA was determined at room temperature (22 °C) from membrane area (via image scanning), thickness (547-400S micrometer, Mitutoyo, Japan), and weight measurements (XPE204, Mettler Toledo, Columbia, SC, USA). Three pieces of 6FDA-mPDA film of 50 microns and three pieces of 240 microns were measured with fresh samples (i.e., 0 days aging). The geometric density of 6FDA-mPDA was 1.42 ± 0.02 g/cm^3. Moreover, the density of 240-μm thick 6FDA-mPDA films aged for >3 months was identical to that of the fresh film samples. This value was slightly lower than other values reported in the literature—that is, 1.464 g/cm^3 [36], 1.46 g/cm^3 [37,38], 1.456 ± 0.014 g/cm^3 [28], and 1.45 ± 0.01 g/cm^3 [39], which were measured via the Archimedes' principle procedure.

Certified gas mixtures of 11 mol% and 90 mol% CO_2 in CH_4 were purchased from Air Liquide; gas mixtures of 37 mol% and 51 mol% CO_2 in CH_4 were purchased from AHG Specialty Gas Center (Jeddah, Saudi Arabia).

2.2. Methods

2.2.1. Barometric System

The design and operation of the system used for barometric pure- and mixed-gas sorption experiments were introduced in detail elsewhere [11] and are shown here in Figure 2. In brief, gases are introduced from volume V_B to V_A, which contains the polymer sample (V_P). Volume V_C is connected to V_A, V_B, the gas chromatograph (GC, Agilent 490 Micro GC Natural Gas Analyzer, Santa Clara, USA), gas cylinders (custom-made mixtures and carrier gas), and a vacuum pump. V_C allows a certain

operational flexibility to this mixed-gas system; for example, by addition from V_C, gases can be mixed in V_B. V_C can receive gas samples from both V_B and V_A for GC analysis. Furthermore, when using custom-made mixtures, the valve between V_B and V_C can be left open to increase the volume of the feed chamber so that more gas can be expanded to V_A. P_A and P_B transducers of 35 atm range were used for both volumes V_A and V_B and were exchanged with transducers of 50 and 100 atm range, respectively, to explore high partial pressures (>15 atm partial gas pressure).
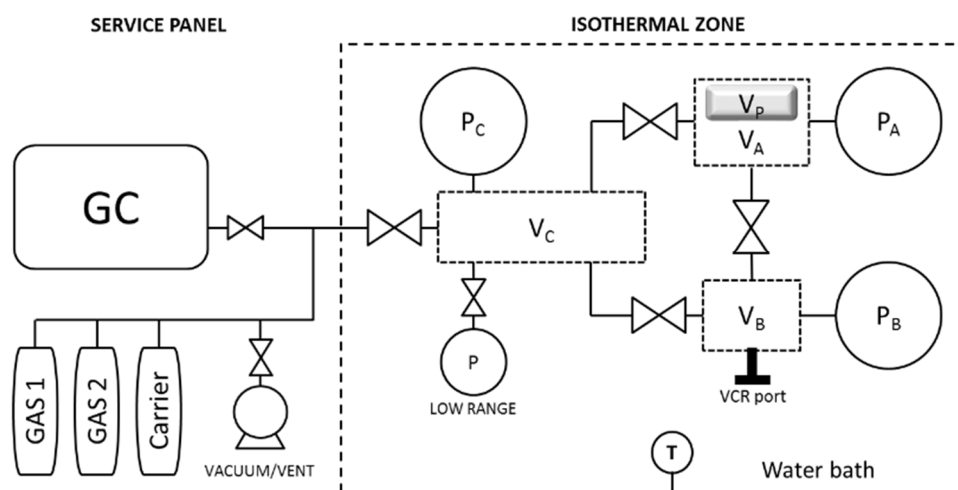

Figure 2. Schematic of the barometric mixed-gas unit used for sorption experiments discussed in this work (adapted from the literature [11]). GC—gas chromatograph.

Active volumes in a barometric sorption system are the feed and the sample chamber because they are used to calculate gas uptakes by mass balance. Dead-volumes in tubes, transducers, and valves do not act actively during sorption experiments. The minimization of these non-active volumes (e.g., by insertion of metallic rods in all tubes [11]) maximizes the difference between amount of *i*-gas in V_A at time zero (i.e., immediately after gas is expanded from V_B to V_A) and the same amount at equilibrium; therefore, volume optimization increments the sensitivity of the mixed-gas sorption system and it was crucial to explore the low solubility coefficient of 6FDA-mPDA toward methane at high partial pressures (see later in this work). All volumes of the pressure-decay system were calibrated via a gas expansion procedure (V_A = 9.00 ± 0.03 cm^3; V_B = 7.77 ± 0.03 cm^3; Vc = 10.44 ± 0.04 cm^3), already well described in the literature [9–14], in which a known reservoir volume, which was previously calibrated via water filling at room temperature, is added to V_A (or eventually to V_B). To the best data accuracy, all volume values employed reflected the actual situation of the system—that is, any maintenance-operation on the system was always followed by a leak-test and a re-calibration procedure, and were always very close to the first calibration values.

2.2.2. Barometric Pure-Gas Sorption

CH_4 and CO_2 barometric pure-gas sorption experiments were performed in the system shown in Figure 2. A fresh film sample of 1.16 g was loaded and degassed for 24 h at 35 °C. Gas was admitted in V_B and was expanded after pressure equilibration to V_A. Data were acquired continuously at a rate of one point every two seconds using custom-made software operating in LabVIEW (National Instruments™, Austin, USA) until the average pressure variation was approximately -2×10^{-7} atm/s during 100 min; above this pressure, variation value uptakes were constant. At equilibrium, more gas was added to V_B and expanded to V_A.

Gas uptakes were estimated as reported previously in the literature [12–15] from the difference between the amount gas first admitted to V_A at time zero and the amount of the same gas not sorbed by the polymer sample at equilibrium. Molar amounts were calculated via the equation of state of gases

(corrected with compressibility factor) from pressure transducer readings. The Soave-Redlich-Kwong (S-R-K) equation of state [40,41] was used to estimate compressibility factors (S-R-K compressibility factors matched with values obtained via the virial equation of state [19]) and partial gas fugacities. The S-R-K parameters of CO_2 and CH_4 can be found elsewhere [15].

The well-established dual-mode sorption (DMS) model [42] was used to fit CH_4 and CO_2 pure-gas uptake data. Because DMS model interpolation of gas uptake from fitted isotherms is usually very accurate, the DMS model was also used for estimation of CO_2 and CH_4 solubilities at infinite dilution of 6FDA-mPDA and other polymers discussed in this work (see Supporting Information).

2.2.3. Gravimetric Gas Sorption

Pure-gas sorption experiments were performed via an Intelligent Gravimetric Analyzer (IGA) by Hiden Isochema (Warrington, UK). A fresh sample was loaded in this gravimetric system and degassed at 35 °C under high vacuum ($<10^{-7}$ mbar) for at least 24 h. When the sample weight was stable, sorption measurements were initiated; gas was introduced in the sample chamber at a rate of 0.1 atm/min to reach the desired equilibrium pressure. After equilibration, gas was added cumulatively to obtain a further pressure point.

2.2.4. Barometric Mixed-Gas Sorption and Data Analysis

To perform mixed-gas sorption experiments (see system in Figure 2), the constant feed concentration procedure described in our previous work [11] was applied. In the framework of this procedure, custom-made mixtures were added to V_B and, after pressure equilibration, expanded to V_A. It should be noted that during this expansion procedure, the valve between A and B volumes was opened and then immediately closed to avoid any interaction between the feed gas in V_B and the gas of V_A now sorbing into the polymer sample (hence, we can assume that at time zero, V_A and V_B have the same gas composition). At sorption equilibrium (i.e., average pressure variation approximately -2×10^{-7} atm/s during 100 minutes), two gas samples from V_B and V_A were sent to V_C for GC analysis. Then, both V_B and V_A were degassed for a time long enough (about the same time allowed for sorption) to remove any sorbed (detectable) gas from the polymer sample in V_A; the 6.8 atm range transducer—mounted on V_C (see "low range" in Figure 2)—was used to detect gas desorption. If no desorption could be detected, the same gas mixture was added at a higher pressure to V_B and then expanded to V_A to perform the next mixed-gas uptake experiment. Once an experimental series at fixed mixture composition reached the highest total feed pressure allowed by V_B (which depended on the maximum value of gas-cylinder pressure, P_B transducer pressure range, and V_B dimension), the next experimental series was carried out from a feed pressure of 7 atm. It should be noted that although we set the sequence of the concentration series in the direction of increasing CO_2 concentrations (i.e., mixtures of higher methane concentration were run first), the sample might have undergone CO_2-conditioning when going from the last pressure of a series to the first experiment of the new series. This sample conditioning might have introduced a certain over-estimation of a few gas uptake data points; however, we anticipate that this effect was relatively small because between two consecutive experimental data points, the difference in CO_2 partial pressure was always lower than 8 atm, and because of the extensive sample degassing mentioned above between each experiment. Mixed-gas uptakes were calculated via mass balance and GC composition data [12–15].

Unless otherwise stated (see Table S4), the same sample used for pure-gas sorption uptakes was employed during mixed-gas sorption experiments.

CO_2 and CH_4 mixed-gas sorption uptakes in 6FDA-mPDA in the form of three-dimensional data points were fitted via MATLAB® software (version R2016b, The MathWorks, Inc, Natick, MA, USA). All data were linearly interpolated or were fitted via the DMS model for mixtures [35] supported by an empirical equation for better data fitting. All details of this fitting analysis can be found in the Supporting Information of this work.

2.2.5. Pure- and Mixed-Gas Permeation and Diffusion Coefficients

Pure- and mixed-gas concentration-averaged effective diffusion coefficients for the case of 50:50 mol% CO_2/CH_4 feed concentration were calculated as previously done elsewhere [14,24,26,27,43] from $\overline{D}_i = P_i/S_i^{feed}$; where P_i is the pure- or mixed-gas permeability at permeate pressures approaching zero, these permeabilities were previously published by our research group for 6FDA-mPDA [29], and S_i^{feed} is the pure- or mixed-gas solubility coefficient of the i-gas at the feed pressure. Because our experimental mixed-gas solubility coefficients were obtained via *constant feed concentration* experiments (i.e., we could only control the concentration at the beginning of the experiment and not at equilibrium [11]), we used models to predict the S_i^{feed} values at the fixed 50:50 mol% CO_2/CH_4 equilibrium concentration. We predicted these values in two ways: (i) with a modified version of the dual-mode sorption model (details can be found in the Supporting Information), and (ii) with the use of the '*linearinterp*' model within the '*fit*' function of Matlab R2016b. The '*linearinterp*' model simply connects all data points of the 3D uptake diagrams with planes (see Figure S5), therefore, the quality of the prediction of S_i^{feed} strictly depends on the number of data points and on experimental accuracy. Both prediction methods for S_i^{feed} produced very similar values (see later in the Results and Discussion section).

3. Results and Discussion

3.1. Experimental Pure- and Mixed-Gas Sorption Data

To assess the effects of multicomponent gas sorption on the sorption capacity of the individual mixture components, pure-gas sorption experiments were first performed by barometric and gravimetric techniques. Pure-gas sorption isotherms obtained via the barometric system with a 6FDA-mPDA film were in excellent agreement with those determined gravimetrically (this comparison validated our instrument accuracy) using film and powder samples (Figure 3a,b), indicating that sorption did not depend on the physical state of the 6FDA-mPDA samples.
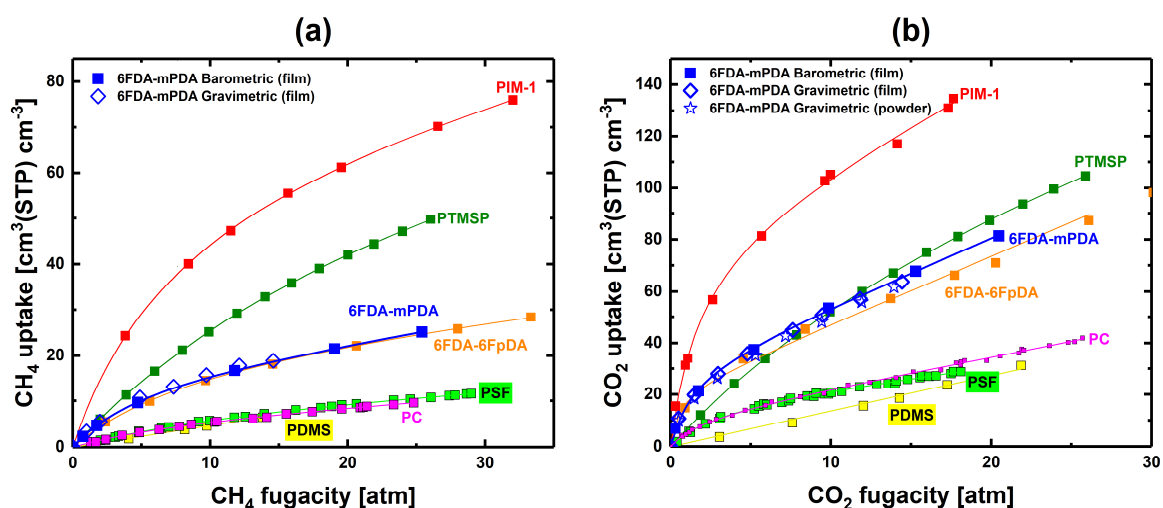

Figure 3. (**a**) CH_4 and (**b**) CO_2 pure-gas sorption isotherms at 35 °C vs. gas fugacity. Blue squares were obtained with 6FDA-mPDA films in our custom-built barometric system. Blue diamonds were obtained with 6FDA-mPDA films via gravimetric sorption. CO_2 pure-gas gravimetric sorption was also performed with a 6FDA-mPDA powder sample (blue stars). Sorption isotherms for polydimethylsiloxane (PDMS) [11], polysulfone (PSF) [45], polycarbonate (PC) [42,46], 6FDA-6FpDA polyimide [44], poly [1-trimethylsilyl-1-propyne] (PTMSP) [15], and polymers of intrinsic microporosity (PIM)-1 [20] are also shown. Interpolations were performed via the dual-mode sorption (DMS) model [42]—DMS parameters were determined in-house. PDMS uptakes were interpolated linearly.

Figure 3 shows that the 6FDA-mPDA polyimide follows the general pure-gas sorption behavior of another fluorine-containing polyimide, that is, the 6FDA-6FpDA [44] (Figure 3a,b). CO_2 and CH_4 isotherms of 6FDA-mPDA are located between the curves of low-free-volume glassy polymers, PSF (polysulfone) and PC (polycarbonate), and high-free-volume PIM-1. The CH_4 sorption uptake in high-free-volume glassy PTMSP is much higher than in 6FDA-mPDA, as shown in Figure 3a. However, CO_2 uptakes are comparable for PTMSP and 6FDA-mPDA (Figure 3b). Hence, this example shows how gas/polymer affinity, as well as free volume, plays an important role in gas sorption.

The CO_2-CH_4 mixed-gas solubility coefficient data for 6FDA-mPDA as function of gas fugacity are shown in Figure 4 (all data are also listed in Table S4). The presence of CO_2 strongly influenced the solubility of CH_4 (Figure 4a), and, similarly but less markedly, CH_4 also affected CO_2 solubility (Figure 4b). The inserts in Figure 4 show the predictions of the extension to mixtures of the dual-mode sorption model (DMS-mix [35]) for CH_4 and CO_2, respectively—these inset graphs are intended to provide a reference framework and to guide the reader through the mixed-gas data. The qualitative agreement between predictions of the DMS model and experiments (Figure 4) suggests that competitive sorption in the glassy polymer may be the *main* reason of the deviation of the mixed-gas data from the pure-gas solubility coefficient trends. Other effects that are not accounted for by the DMS model and that impact solubility at high pressures are presented in the Supporting Information of this paper.
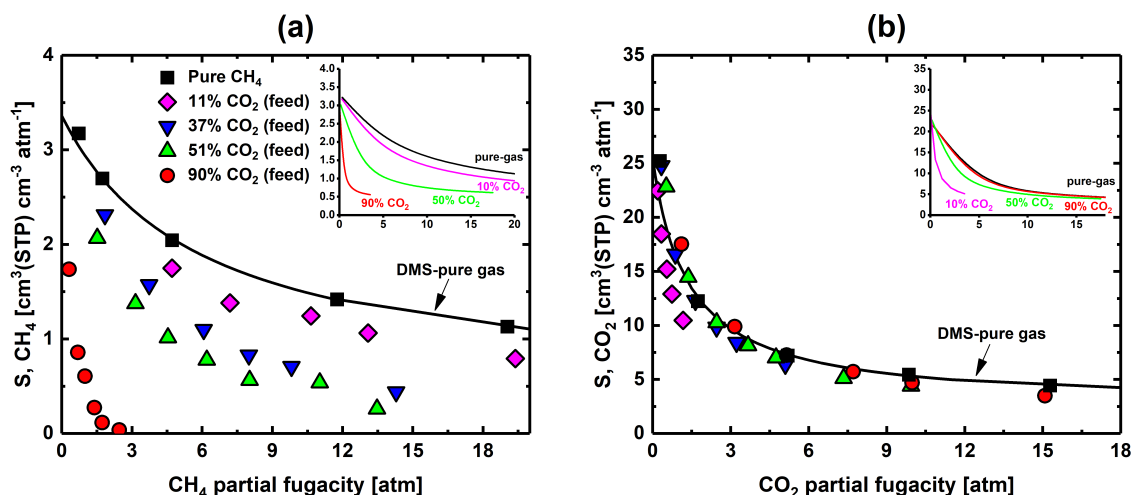

Figure 4. (**a**) Experimental CH_4 solubility coefficient vs. CH_4 fugacity and (**b**) CO_2 solubility coefficient vs. CO_2 fugacity of 6FDA-mPDA. The inset graphs report the solubility coefficient behavior of CH_4 and CO_2 at various equilibrium concentrations—these curves were predicted using the dual-mode sorption model extended to mixtures (DMS-mix) [35] and the pure-gas DMS sorption parameters (Table S1). Note that the feed mixture concentration is the parameter for the experimental data in (**a**,**b**), whereas the concentration at equilibrium is the parameter for the DMS-mix predictions (insert graphs); hence, the comparison between experimental data and predictions is qualitative (i.e., the DMS-mix curves guide the reader through the data).

Because 6FDA-mPDA has strong affinity to CO_2, and hence high sorption uptake, the experimental data exhibit small scattering. Conversely, solubility coefficients of methane were scattered at low CH_4 feed concentrations and at high total pressures, because the accuracy limit of the system was approached (methane solubility coefficients lower than ~0.5 cm^3(STP) cm^{-3} atm^{-1} require volumes optimization of the barometric pressure decay system, as discussed elsewhere [11]).

3.2. Solubility Selectivity Analysis

We further analyzed our experimental results of mixed-gas solubility for 6FDA-mPDA via a plot of CO_2 mixed-gas solubility coefficient versus CH_4 mixed-gas solubility coefficient (Figure 5a). Note that each mixed-gas sorption experiment produces two solubility coefficients: one for CO_2 and one

for CH_4; hence, these two solubility coefficients generate a single data point in the plot of Figure 5a. Experimental mixed-gas solubility coefficient data at 35 °C are also shown from previous studies for PIM-1 [20], TZ-PIM-1 [23], PTMSP [15], and PPO [18]—data of AO-PIM-1 [23] and polynonene [23] are plotted in Figure S1. Interestingly, all experimental data could be fitted with a straight line regardless of mixture concentration.

The straight line fitted to the data in Figure 5a follows the following equation:

$$S_{CO_2} = \alpha^o_{CO_2/CH_4} \cdot S_{CH_4} + B \tag{1}$$

where S_{CO_2} and S_{CH_4} are the solubility coefficient of CO_2 and CH_4, respectively; $\alpha^o_{CO_2/CH_4}$ is the mixed-gas selectivity at infinite dilution, that is, the slope of the straight line; and B is the intercept. We rearranged this equation as follows:

$$\alpha^{mix,S}_{CO_2/CH_4} = \frac{S_{CO_2}}{S_{CH_4}} = \alpha^o_{CO_2/CH_4} + \frac{B}{S_{CH_4}} \tag{2}$$

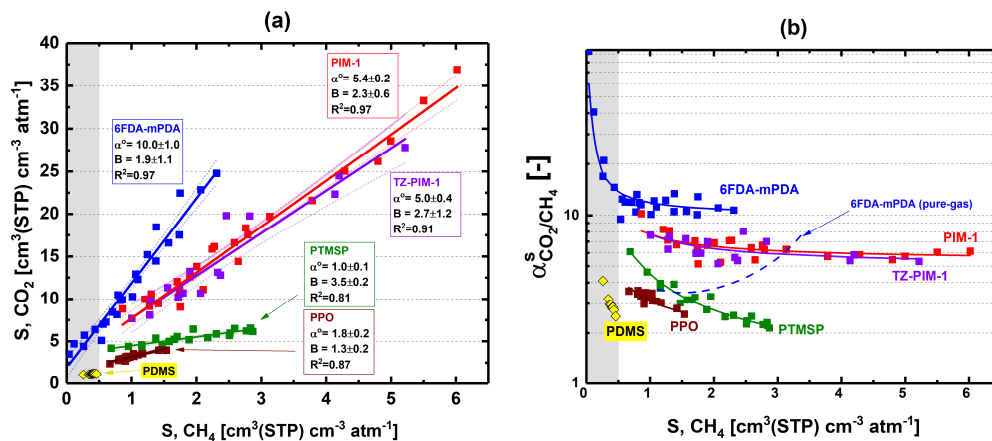where $\alpha^{mix,S}_{CO_2/CH_4}$ is the mixed-gas solubility selectivity coefficient of the membrane material.

Figure 5. (**a**) CO_2 vs. CH_4 mixed-gas solubility coefficient of 6FDA-mPDA at 35 °C—solid lines were estimated via linear fitting of experimental data (the dotted curves delimit the confidence intervals of each linear interpolation); (**b**) data of CO_2/CH_4 mixed-gas solubility selectivity vs. CH_4 mixed-gas solubility coefficient of 6FDA-mPDA (CO_2/CH_4 mixed-gas solubility selectivity vs. CH_4 mixed-gas solubility coefficient mixed- (solid line) and pure-gas trends (dashed-line) are also shown for comparison). Mixed-gas solubility coefficient data from previous reports on PDMS [11], PIM-1 [20], TZ-PIM-1 [23], PTMSP [15], and PPO [18] are included in (**a**,**b**).

When S_{CH_4} is high, and $\frac{B}{S_{CH_4}} \ll \alpha^o_{CO_2/CH_4}$, $\alpha^{mix,S}_{CO_2/CH_4} = \alpha^o_{CO_2/CH_4}$ (Equation (2)); this condition may be found for very low equilibrium pressures. Hence, $\alpha^o_{CO_2/CH_4}$ corresponds to the ratio between the solubility coefficient of CO_2 and CH_4 at infinite dilution. For most of the polymers shown in Figure 5a, the pure-gas solubility selectivity at infinite dilution (estimated via the DMS model in the form of Equation S2) was in good agreement with the experimental values found via linear interpolation of CO_2 mixed-gas solubility coefficient versus CH_4 mixed-gas solubility coefficient data (i.e., $\alpha^o_{CO_2/CH_4}$); this comparison is discussed in the Supporting Information of this work. When S_{CH_4} is low (i.e., for high equilibrium pressures), a second limiting condition is found; in this case, the CO_2/CH_4 solubility selectivity diverges positively from the $\alpha^o_{CO_2/CH_4}$ value if $B > 0$.

The significance of B and $\alpha^o_{CO_2/CH_4}$ in Equations (1) and (2) can be better appreciated in Figure 5b, where the mixed-gas solubility selectivity of 6FDA-mPDA, PIM-1, TZ-PIM-1, PTMSP, PPO, and the predictions of Equation (2) are plotted against the solubility coefficient of CH_4. For all polymers, predictions by Equation (2) follow the experimental data, and as S_{CH_4} decreases, the mixed-gas

solubility selectivity increases ($B > 0$)—especially in the grey region of Figure 5. Note that during linear fitting of CO_2 versus CH_4 mixed-gas solubilities of 6FDA-mPDA (Figure 5a), the data in the grey region had almost no influence on $\alpha^o_{CO_2/CH_4}$, while they could affect the value of B, but not the sign—this confirms the overall trends of solubility selectivity shown in Figure 5b. Interestingly, the mixed-gas data of rubbery PDMS [11] also follow the trend seen for 6FDA-mPDA.

In Figure 5b, the solubility selectivity increases with pressure ($B > 0$) from $\alpha^o_{CO_2/CH_4}$; hence, $\alpha^o_{CO_2/CH_4}$ appears to be a characteristic solubility selectivity value of glassy polymers. We plotted data of $\alpha^o_{CO_2/CH_4}$ versus CO_2 solubility coefficient at infinite dilution in the 2014 upper bound solubility plot (Figure 6) discussed by Lou et al. [47]. The solubility selectivity at infinite dilution of AO-PIM-1 was obtained from pure-gas uptake experiments (see Supporting Information). For both PTMSP and PPO, the solubility selectivity at infinite dilution estimated from Equation (2) and from the DMS model (i.e., from the ratio of DMS solubility coefficients at infinite dilution calculated via Equation S2) did not agree within the respective standard deviations and were both plotted in Figure 6. The values of $\alpha^o_{CO_2/CH_4}$ and CO_2 solubility coefficient at infinite dilution for 6FDA-TADPO were uncertain, because of the limited number of pure- and mixed-gas data reported [22,48]. Although the standard error is very large, the pure-gas 6FDA-TADPO solubility trend is qualitatively similar to 6FDA-mPDA (Figure 6). Similarly, PIM-1, TZ-PIM-1, and AO-PIM-1 points group in a confined region of the 2014 CO_2/CH_4 solubility upper bound plot.
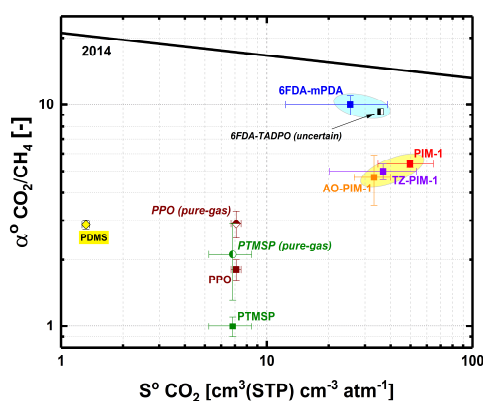

Figure 6. CO_2 solubility coefficient vs. CO_2/CH_4 solubility selectivity (at infinite dilution) data of all polymers tested for CO_2-CH_4 mixed-gas sorption at 35 °C [11,15,18,20,22,23,48]. CO_2/CH_4 solubility selectivities were obtained from linear interpolation of CO_2 mixed-gas solubility coefficient vs. CH_4 mixed-gas solubility coefficient data or from pure-gas uptake data via DMS model equations—see the discussion in the Supporting Information and data values in Table S2. CO_2 solubility coefficients were estimated from experimental data of pure-gas CO_2 uptake. The 2014 CO_2/CH_4 solubility upper bound was discussed elsewhere [47].

3.3. Equimolar CO_2-CH_4 Mixed-Gas Diffusion

To elucidate the phenomena that affect the separation performance of 6FDA-mPDA polyimide in mixed-gas conditions, we first show previously reported pure- and 50 mol% mixed-gas permeability data of 6FDA-mPDA from our group [29]—here, these data were corrected with fugacity coefficients and re-plotted in Figure 7. Secondly, we incorporate the results of our pure- and mixed-gas solubility experiments to clarify the contribution of mixed-gas solubility to permeability. Finally, CH_4 and CO_2 pure- and mixed-gas concentration-averaged effective diffusion coefficients are discussed.

After correction of partial pressures and driving forces with fugacity coefficients, permeability trends show that CO_2 mixed-gas permeability suffers from the presence of methane (a local minimum is found at about ~10 atm partial fugacity), whereas CH_4 mixed-gas permeability increases in mixed-gas conditions, particularly above ~10 atm partial fugacity (Figure 7a). Overall, the permeability selectivity of the mixture strongly diverges from the pure-gas trend (Figure 7b); at about 18 atm partial fugacity,

almost 35% of the ideal permeability selectivity is lost. Frequently, it is assumed that competitive sorption is the cause for this loss of permeability selectivity. The data of mixed-gas solubilities at 50 mol% equilibrium concentration (Figure 8) show that competitive sorption strongly affects CH_4 mixed-gas solubility—that is, when partial pressures increase, the CH_4 mixed-gas solubility coefficients diverge from the pure-gas values. Because the effect of competitive sorption on the solubility coefficient of CO_2 is limited, we found that at 2 atm CO_2 partial pressure, the CO_2/CH_4 solubility selectivity jumps from a value of ~5 in the pure-gas state to ~10 in the mixture; moreover, as previously discussed, the CO_2/CH_4 mixed-gas solubility selectivity increases with partial pressures. Thus, the effects of gas mixture on solubility selectivity are beneficial during separation of CO_2 from CH_4 (equimolar feed) and cannot be held responsible for the loss of permeability selectivity from ideality (Figure 7b).
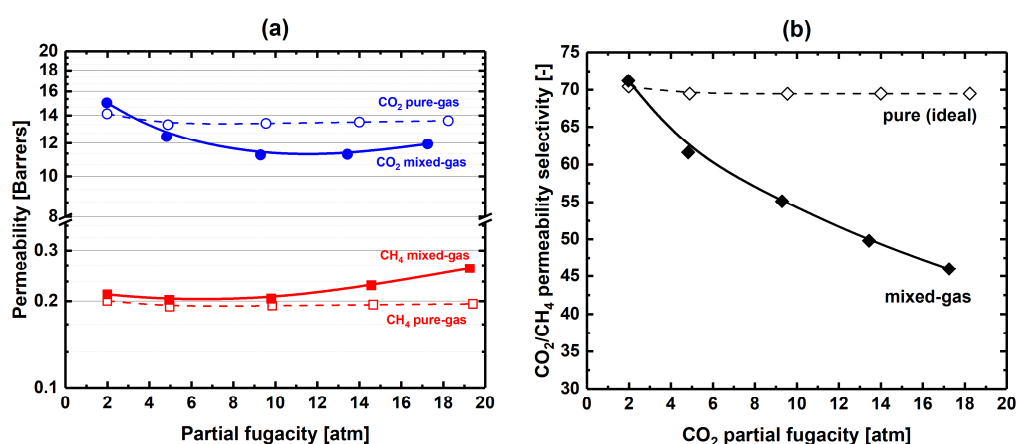

Figure 7. (**a**) CH_4 and CO_2 pure- and mixed-gas permeability data (6FDA-mPDA) vs. partial fugacities; (**b**) CO_2/CH_4 pure- and mixed-gas permeability selectivity data vs. CO_2 partial fugacities (feed was equimolar). CH_4 and CO_2 permeabilities based on partial pressures were previously reported by our group [29] and corrected with fugacity coefficients. Lines are drawn to guide the eye.
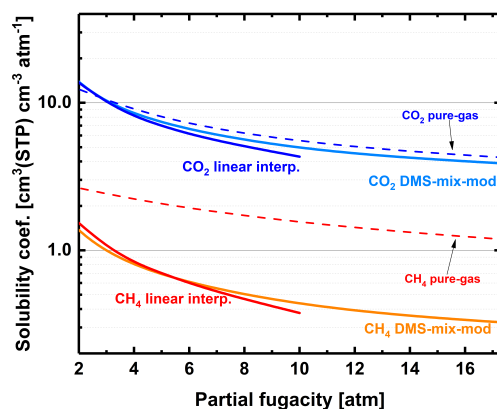

Figure 8. CH_4 and CO_2 pure- and mixed-gas solubility coefficients (6FDA-mPDA) vs. partial fugacities. The mixed-gas solubility coefficient curves for methane and carbon dioxide were obtained by linear interpolations of mixed-gas experimental data or by fitting with a modified version of the DMS model for gas mixtures (DMS-mix-mod)—more details can be found in the Supporting Information of this work (Figure S4 and Figure S5).

Hence, kinetic effects must be responsible for the deviation of mixed-gas permeability selectivity from the pure-gas values. Figure 9a shows the variation of pure- and mixed-gas concentration-averaged effective diffusion coefficients with partial fugacities. The mixed-gas diffusivities of CH_4 notably deviate from the pure-gas trend, whereas CO_2 diffuses in the same manner in pure- and mixed-gas environments with almost no disturbance by methane (Figure 9a). The CO_2/CH_4 mixed-gas diffusion

selectivity drops from an average pure-gas value of ~18 to a mixed-gas value of ~5 (Figure 9b), simply because in the mixture, CH_4 diffusion is enhanced compared with that in the pure-gas environment because of the presence of CO_2 in the mixture. Similar effects on CO_2-CH_4 diffusion were observed for PDMS rubber [11]; in this case, sorption of CO_2 induced the decline of the mixed-gas diffusion and permeability selectivity relative to the pure-gas values. A similar case was discussed by Ribeiro et al. [24], who described how the increase of C_2H_6 mixed-gas diffusion coefficient and the decrease of the CO_2/C_2H_6 permeability selectivity could be ascribed to CO_2-induced "plasticization" of a XLPEO rubber film.

Finally, from the analysis of the data in Figure 7a, one may conclude that "plasticization" of 6FDA-mPDA takes place at partial fugacities greater than ~10 atm, where the gas permeability shows minima for both CO_2 and CH_4. However, CH_4 mixed-gas diffusion rises immediately at low feed pressure after the polymer matrix sorbs CO_2 (Figure 9a); in other words, the effect of CO_2 sorption on gas transport occurs over the entire range of partial pressures explored in this work, and the local minima seen in Figure 7a were produced by counteracting thermodynamic and kinetic contributions to transport.
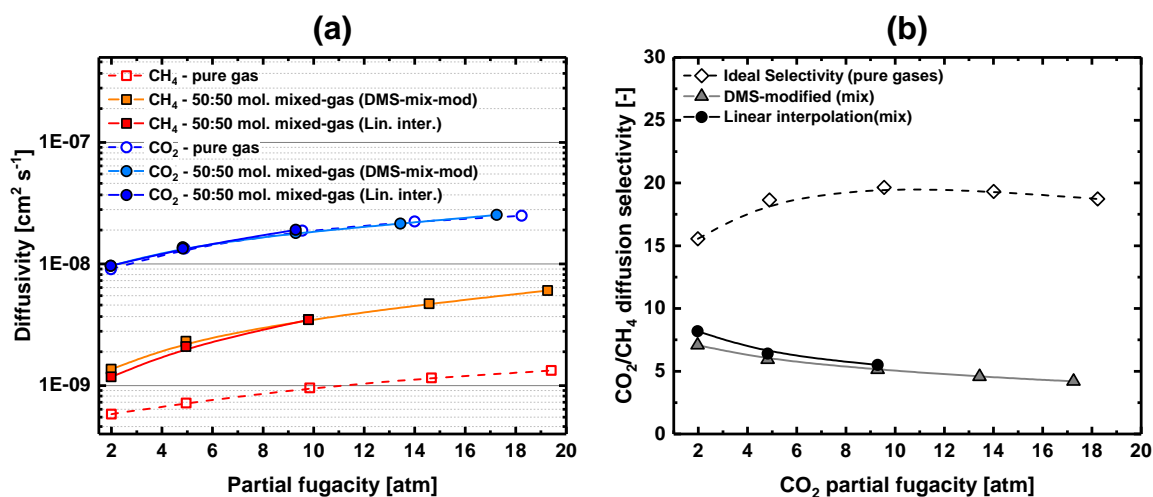

Figure 9. (**a**) CH_4 and CO_2 pure- and mixed-gas diffusion coefficients (6FDA-mPDA) vs. partial fugacity; (**b**) CO_2/CH_4 pure- and mixed-gas diffusion selectivity vs. CO_2 partial fugacity. Lines are drawn to guide the eye.

4. Conclusions

To quantify the deviation from ideality of CO_2-CH_4 mixed-gas permeability and CO_2/CH_4 mixed-gas permeability selectivity of 6FDA-mPDA at 35 °C, sorption and diffusion contributions to permeation were decoupled. Experimental data of mixed-gas solubility revealed a decrease of both CO_2 and, more markedly, CH_4 solubility due to mixture effects. We found that CO_2 versus CH_4 mixed-gas solubility coefficients of 6FDA-mPDA (and other glassy polymers previously studied) follow a linear trend regardless of equilibrium concentration. The slope of the trend line agrees well with the CO_2/CH_4 solubility selectivity at infinite dilution, and the intercept indicates the way in which solubility selectivity deviates at increasing pressures. We found the same behavior reviewing mixed-gas sorption data of glassy polymers reported in the literature. In all cases, the CO_2/CH_4 solubility selectivity increases with pressure from the value of solubility selectivity at infinite dilution.

Because the CO_2/CH_4 solubility selectivity of 6FDA-mPDA improved under mixed-gas conditions, the decline of CO_2/CH_4 mixed-gas permeability selectivity from the corresponding pure-gas permeability selectivities—typically observed during CO_2-CH_4 permeation in polymeric films—could not be attributed to competitive sorption (as frequently assumed in the literature). Hence, we studied the kinetic behavior of 6FDA-mPDA to elucidate the effect of gas mixture effects on

concentration-averaged effective diffusion coefficients as estimated from experimental mixed-gas sorption and permeation data. We observed that after CO_2 was added to CH_4 in a mixture, even at a low concentration, the concentration-averaged effective diffusion coefficient of CH_4 deviated from the pure-gas values, whereas the concentration-averaged effective diffusion coefficient of CO_2 essentially followed the pure-gas trend; hence, the departure of CO_2/CH_4 permeability selectivity of 6FDA-mPDA from the pure-gas values can be explained by a depression of the size sieving capability of 6FDA-mPDA (i.e., it makes CH_4 diffusion faster than in the pure-gas environment) induced by the presence of CO_2 by sorption in the polymeric film matrix.

Supplementary Materials: The following are available online at http://www.mdpi.com/2077-0375/9/1/10/s1. Figure S1: Data of CO_2 mixed-gas solubility vs. CH_4 mixed-gas solubility coefficient of AO-PIM-1 and polynonene [2]. For both interpolations, the slope was fixed at the value of pure-gas solubility selectivity at infinite dilution. For both interpolations, the slope was fixed at the value of pure-gas solubility selectivity at infinite dilution. Figure S2: In red and in blue, two examples of the behavior of the *switch* function (Equation S5) used in this work to track the behavior of K_{Di} and b_i parameters. In this graph, $A_i^{pure} = 1$. Figure S3: Comparison between experimental uptakes and model predictions for (a) CH_4 and (b) CO_2. Black squares are predictions of the DMS-mix with pure-gas parameters. Red circles are predictions of the DMS-mix-mod. Figure S4: CH_4 (a) and CO_2 (b) mixed-gas uptakes in 6FDA-mPDA. Surfaces were obtained via the DMS-mix-mod fitting. The DMS-mix-mod allowed us to predict the solubility behavior beyond the region covered by experimental data. Figure S5: CH_4 (a) and CO_2 (b) mixed-gas uptakes in 6FDA-mPDA. Surfaces were obtained via linear interpolation. Table S1: Dual-mode model parameters of methane and carbon dioxide in 6FDA-mPDA for pure-gas sorption at 35 °C. Table S2: Comparison between solubility selectivities at infinite dilution retrieved from mixed-gas and pure-gas sorption data. Table S3: Parameters derived from DMS-mix-mod fitting. Table S4: Pure- and mixed-gas uptake data presented in this work.

Author Contributions: Conceptualization, I.P. and G.G.; methodology, I.P. and G.G.; investigation, G.G.; data acquisition, G.G.; writing—original draft preparation, G.G.; review and editing, I.P.; polymer synthesis, B.S.G.

Conflicts of Interest: The authors declare no conflict of interest.

References

1.   Sholl, D.S.; Lively, R.P. Seven chemical separations to change the world. *Nature* **2016**, *532*, 435–438. [CrossRef] [PubMed]

2.   Budd, P.M.; Msayib, K.J.; Tattershall, C.E.; Ghanem, B.S.; Reynolds, K.J.; McKeown, N.B.; Fritsch, D. Gas separation membranes from polymers of intrinsic microporosity. *J. Membr. Sci.* **2005**, *251*, 263–269. [CrossRef]

3.   Swaidan, R.; Ma, X.; Litwiller, E.; Pinnau, I. High pressure pure- and mixed-gas separation of CO_2/CH_4 by thermally-rearranged and carbon molecular sieve membranes derived from a polyimide of intrinsic microporosity. *J. Membr. Sci.* **2013**, *447*, 387–394. [CrossRef]

4.   Swaidan, R.; Ghanem, B.S.; Litwiller, E.; Pinnau, I. Pure- and mixed-gas CO_2/CH_4 separation properties of PIM-1 and an amidoxime-functionalized PIM-1. *J. Membr. Sci.* **2014**, *457*, 95–102. [CrossRef]

5.   Sanders, D.F.; Smith, Z.P.; Guo, R.; Robeson, L.M.; McGrath, J.E.; Paul, D.R.; Freeman, B.D. Energy-efficient polymeric gas separation membranes for a sustainable future: A review. *Polymer* **2013**, *54*, 4729–4761. [CrossRef]

6.   Puleo, A.C.; Paul, D.R.; Kelley, S.S. The effect of degree of acetylation on gas sorption and transport behavior in cellulose acetate. *J. Membr. Sci.* **1989**, *47*, 301–332. [CrossRef]

7.   Wijmans, J.G.; Baker, R.W. The solution-diffusion model: A review. *J. Membr. Sci.* **1995**, *107*, 1–21. [CrossRef]

8.   O'Brien, K.C.; Koros, W.J.; Barbari, T.A.; Sanders, E.S. A new technique for the measurement of multicomponent gas transport through polymeric films. *J. Membr. Sci.* **1986**, *29*, 229–238. [CrossRef]

9.   Fraga, S.C.; Monteleone, M.; Lanč, M.; Esposito, E.; Fuoco, A.; Giorno, L.; Pilnáček, K.; Friess, K.; Carta, M.; McKeown, N.B.; et al. A novel time lag method for the analysis of mixed gas diffusion in polymeric membranes by on-line mass spectrometry: Method development and validation. *J. Membr. Sci.* **2018**, *561*, 39–58. [CrossRef]

10. Monteleone, M.; Esposito, E.; Fuoco, A.; Lanč, M.; Pilnáček, K.; Friess, K.; Bezzu, C.G.; Carta, M.; McKeown, N.B.; Jansen, J.C. A novel time lag method for the analysis of mixed gas diffusion in polymeric

membranes by on-line mass spectrometry: Pressure dependence of transport parameters. *Membranes* **2018**, *8*, 73. [CrossRef]

11. Genduso, G.; Litwiller, E.; Ma, X.; Zampini, S.; Pinnau, I. Mixed-gas sorption in polymers via a new barometric test system: Sorption and diffusion of CO_2-CH_4 mixtures in polydimethylsiloxane (PDMS). Manuscript submitted for publication.

12. Koros, W.J.; Paul, D.R. Design considerations for measurement of gas sorption in polymers by pressure decay. *J. Polym. Sci. Polym. Phys. Ed.* **1976**, *14*, 1903–1907. [CrossRef]

13. Ribeiro, C.P.; Freeman, B.D. Carbon dioxide/ethane mixed-gas sorption and dilation in a cross-linked poly(ethylene oxide) copolymer. *Polymer* **2010**, *51*, 1156–1168. [CrossRef]

14. Raharjo, R.D.; Freeman, B.D.; Sanders, E.S. Pure and mixed gas CH_4 and *n*-C_4H_{10} sorption and dilation in poly(1-trimethylsilyl-1-propyne). *Polymer* **2007**, *48*, 6097–6114. [CrossRef]

15. Vopička, O.; De Angelis, M.G.; Sarti, G.C. Mixed gas sorption in glassy polymeric membranes: I. CO_2/CH_4 and *n*-C_4/CH_4 mixtures sorption in poly(1-trimethylsilyl-1-propyne) (PTMSP). *J. Membr. Sci.* **2014**, *449*, 97–108. [CrossRef]

16. Sanders, E.S.; Koros, W.J.; Hopfenberg, H.B.; Stannett, V.T. Mixed gas sorption in glassy polymers: Equipment design considerations and preliminary results. *J. Membr. Sci.* **1983**, *13*, 161–174. [CrossRef]

17. Sanders, E.S.; Koros, W.J.; Hopfenberg, H.B.; Stannett, V.T. Pure and mixed gas sorption of carbon dioxide and ethylene in poly(methyl methacrylate). *J. Membr. Sci.* **1984**, *18*, 53–74. [CrossRef]

18. Story, B.J.; Koros, W.J. Sorption of CO_2/CH_4 mixtures in poly(phenylene oxide) and a carboxylated derivative. *J. Appl. Polym. Sci.* **1991**, *42*, 2613–2626. [CrossRef]

19. Raharjo, R.D.; Freeman, B.D.; Sanders, E.S. Pure and mixed gas CH_4 and *n*-C_4H_{10} sorption and dilation in poly(dimethylsiloxane). *J. Membr. Sci.* **2007**, *292*, 45–61. [CrossRef]

20. Vopička, O.; De Angelis, M.G.; Du, N.; Li, N.; Guiver, M.D.; Sarti, G.C. Mixed gas sorption in glassy polymeric membranes: II. CO_2/CH_4 mixtures in a polymer of intrinsic microporosity (PIM-1). *J. Membr. Sci.* **2014**, *459*, 264–276. [CrossRef]

21. Gemeda, A.E.; De Angelis, M.G.; Du, N.; Li, N.; Guiver, M.D.; Sarti, G.C. Mixed gas sorption in glassy polymeric membranes. III. CO_2/CH_4 mixtures in a polymer of intrinsic microporosity (PIM-1): Effect of temperature. *J. Membr. Sci.* **2017**, *524*, 746–757. [CrossRef]

22. Kamaruddin, H.D.; Koros, W.J. Some observations about the application of Fick's first law for membrane separation of multicomponent mixtures. *J. Membr. Sci.* **1997**, *135*, 147–159. [CrossRef]

23. Gemeda, A.E. Solubility, Diffusivity and Permeability of Gases in Glassy Polymers. Ph.D. Thesis, Università di Bologna, Bologna, Italy, 2015.

24. Ribeiro, C.P.; Freeman, B.D.; Paul, D.R. Pure- and mixed-gas carbon dioxide/ethane permeability and diffusivity in a cross-linked poly(ethylene oxide) copolymer. *J. Membr. Sci.* **2011**, *377*, 110–123. [CrossRef]

25. Raharjo, R.D.; Freeman, B.D.; Paul, D.R.; Sanders, E.S. Pure and mixed gas CH_4 and *n*-C_4H_{10} permeability and diffusivity in poly(1-trimethylsilyl-1-propyne). *Polymer* **2007**, *48*, 7329–7344. [CrossRef]

26. Reijerkerk, S.R.; Nijmeijer, K.; Ribeiro, C.P.; Freeman, B.D.; Wessling, M. On the effects of plasticization in CO_2/light gas separation using polymeric solubility selective membranes. *J. Membr. Sci.* **2011**, *367*, 33–44. [CrossRef]

27. Raharjo, R.D.; Freeman, B.D.; Paul, D.R.; Sarti, G.C.; Sanders, E.S. Pure and mixed gas CH_4 and *n*-C_4H_{10} permeability and diffusivity in poly(dimethylsiloxane). *J. Membr. Sci.* **2007**, *306*, 75–92. [CrossRef]

28. Tanis, I.; Brown, D.; Neyertz, S.J.; Heck, R.; Mercier, R. A comparison of homopolymer and block copolymer structure in 6FDA-based polyimides. *Phys. Chem. Chem. Phys.* **2014**, *16*, 23044–23055. [CrossRef]

29. Alaslai, N.; Ghanem, B.; Alghunaimi, F.; Litwiller, E.; Pinnau, I. Pure- and mixed-gas permeation properties of highly selective and plasticization resistant hydroxyl-diamine-based 6FDA polyimides for CO_2/CH_4 separation. *J. Membr. Sci.* **2016**, *505*, 100–107. [CrossRef]

30. Qiu, W.; Zhang, K.; Li, F.S.; Zhang, K.; Koros, W.J. Gas separation performance of carbon molecular sieve membranes based on 6FDA-mPDA/DABA (3:2) polyimide. *ChemSusChem* **2014**, *7*, 1186–1194. [CrossRef]

31. Gleason, K.L.; Smith, Z.P.; Liu, Q.; Paul, D.R.; Freeman, B.D. Pure- and mixed-gas permeation of CO_2 and CH_4 in thermally rearranged polymers based on 3,3′-dihydroxy-4,4′-diamino-biphenyl (HAB) and 2,2′-bis-(3,4-dicarboxyphenyl) hexafluoropropane dianhydride (6FDA). *J. Membr. Sci.* **2015**, *475*, 204–214. [CrossRef]

32. Swaidan, R.; Ghanem, B.; Litwiller, E.; Pinnau, I. Physical aging, plasticization and their effects on gas permeation in "rigid" polymers of intrinsic microporosity. *Macromolecules* **2015**, *48*, 6553–6561. [CrossRef]

33. Swaidan, R.; Ghanem, B.; Al-Saeedi, M.; Litwiller, E.; Pinnau, I. Role of intrachain rigidity in the plasticization of intrinsically microporous triptycene-based polyimide membranes in mixed-gas CO_2/CH_4 separations. *Macromolecules* **2014**, *47*, 7453–7462. [CrossRef]

34. Staudt-Bickel, C.J.; Koros, W. Improvement of co_2/ch_4 separation characteristics of polyimides by chemical crosslinking. *J. Membr. Sci.* **1999**, *155*, 145–154. [CrossRef]

35. Koros, W.J. Model for sorption of mixed gases in glassy polymers. *J. Polym. Sci. Polym. Phys. Ed.* **1980**, *18*, 981–992. [CrossRef]

36. Comesaña-Gándara, B.; Hernández, A.; de la Campa, J.G.; de Abajo, J.; Lozano, A.E.; Lee, Y.M. Thermally rearranged polybenzoxazoles and poly(benzoxazole-co-imide)s from ortho-hydroxyamine monomers for high performance gas separation membranes. *J. Membr. Sci.* **2015**, *493*, 329–339. [CrossRef]

37. Cheng, S.-X.; Chung, T.-S.; Wang, R.; Vora, R.H. Gas-sorption properties of 6FDA–durene/1,4-phenylenediamine (pPDA) and 6FDA–durene/1,3-phenylenediamine (mPDA) copolyimides. *J. Appl. Polym. Sci.* **2003**, *90*, 2187–2193. [CrossRef]

38. Heck, R.; Qahtani, M.S.; Yahaya, G.O.; Tanis, I.; Brown, D.; Bahamdan, A.A.; Ameen, A.W.; Vaidya, M.M.; Ballaguet, J.P.R.; Alhajry, R.H.; et al. Block copolyimide membranes for pure- and mixed-gas separation. *Sep. Purif. Technol.* **2017**, *173*, 183–192. [CrossRef]

39. Joly, C.; Le Cerf, D.; Chappey, C.; Langevin, D.; Muller, G. Residual solvent effect on the permeation properties of fluorinated polyimide films. *Sep. Purif. Technol.* **1999**, *16*, 47–54. [CrossRef]

40. Redlich, O.; Kwong, J.N.S. On the thermodynamics of solutions. V. An equation of state. Fugacities of gaseous solutions. *Chem. Rev.* **1949**, *44*, 233–244. [CrossRef]

41. Soave, G. 20 years of Redlich-Kwong equation of state. *Fluid Phase Equilib.* **1993**, *82*, 345–359. [CrossRef]

42. Koros, W.J.; Chan, A.H.; Paul, D.R. Sorption and transport of various gases in polycarbonate. *J. Membr. Sci.* **1977**, *2*, 165–190. [CrossRef]

43. Sadrzadeh, M.; Shahidi, K.; Mohammadi, T. Effect of operating parameters on pure and mixed gas permeation properties of a synthesized composite PDMS/PA membrane. *J. Membr. Sci.* **2009**, *342*, 327–340. [CrossRef]

44. Coleman, M.R. Isomers of Fluorine-Containing Polyimides for Gas Separation Membranes. Ph.D. Thesis, The University of Texas at Austin, Austin, TX, USA, 1992.

45. Erb, A.J.; Paul, D.R. Gas sorption and transport in polysulfone. *J. Membr. Sci.* **1981**, *8*, 11–22. [CrossRef]

46. Koros, W.J.; Paul, D.R.; Rocha, A.A. Carbon dioxide sorption and transport in polycarbonate. *J. Polym. Sci. Polym. Phys. Ed.* **1976**, *14*, 687–702. [CrossRef]

47. Lou, Y.; Hao, P.; Lipscomb, G. NELF predictions of a solubility–solubility selectivity upper bound. *J. Membr. Sci.* **2014**, *455*, 247–253. [CrossRef]

48. Walker, D.R.B. Synthesis and Characterization of Polypyrrolones for Gas Separation Membranes. Ph.D. Thesis, The University of Texas at Austin, Austin, TX, USA, 1993.